Continuous High-Accuracy Radio Positioning of Cars in Ultra-Dense 5G Networks

Mike Koivisto*, Aki Hakkarainen*, Mário Costa†, Jukka Talvitie*, Kari Heiska†,
Kari Leppänen†, and Mikko Valkama*
* Laboratory of Electronics and Communications Engineering, Tampere University of Technology, Finland
Emails: {mike.koivisto, aki.hakkarainen, jukka.talvitie, mikko.e.valkama}@tut.fi
† Huawei Technologies Oy (Finland) Co., Ltd, Finland R&D Center
Emails: {mariocosta, kari.heiska, kari.leppanen}@huawei.com

***Abstract*—The upcoming fifth generation (5G) radio networks will be the game changer of future societies. In addition to obvious improvements in wireless communications, 5G enables also highly accurate user equipment (UE) positioning that is carried out on the network side. Such a solution provides ubiquitous positioning services without draining the batteries of the UEs. In this paper, we concentrate on positioning methods that suits the future needs of automotive transportation and intelligent transportation system (ITS). In particular, we demonstrate how location estimates can be obtained in 5G ultra-dense networks (UDNs) efficiently and even in a proactive manner where the UE locations can be predicted to some extent. Numerical performance analysis will then illustrate that the proposed 5G-based network-centric positioning solutions are well-suited for car and traffic applications, providing even sub-meter range positioning accuracy.**

***Index Terms*—5G networks, extended Kalman filter, positioning, prediction, tracking, ultra dense networks**

I. Introduction

Evolution in radio networks has led us from the ages of mobile phone calls to a modern society where data connections are highly available. Fifth generation (5G) networks will continue this progress towards more densely populated networks with, e.g., considerably higher data throughputs and much lower latencies than the existing wireless networks are capable of [1], [2]. However, it is often forgotten that 5G enables improvements also in other areas than merely communications related services. That is, 5G radio networks provide an unforeseen opportunity for network-based user equipment (UE) positioning that allows for further development of existing services as well as creating completely new types of services in many vertical industries [3].

In order to achieve the future needs of sub-meter positioning accuracy [3]–[6], radio positioning in 5G networks is of utterly importance due to the limited capabilities of the existing positioning systems. In particular, global navigation satellite system (GNSS)-based positioning, having an accuracy around $5\,\mathrm{m}$ [7], cause heavy computational burden to the UEs to be positioned thus leading to short battery life of UEs. Moreover, GNSS-based positioning requires visibility to > 3 satellites which is typically challenging in urban environments with high-rise buildings. Network-based positioning is in turn possible with observed time difference of arrival (OTDoA)-based techniques in long term evolution (LTE) networks, but it provides an accuracy of only a couple of tens of meters [8]. Techniques based on wireless local area network (WLAN) fingerprinting are not a solution for achieving the envisioned sub-meter positioning performance either, since their accuracy is typically $3\text{-}4\,\mathrm{m}$ [9], and additionally they require acquisition and maintenance of fingerprint databases. Fortunately, 5G-based radio positioning is expected to be even capable of sub-meter accuracy while the actual computations can be carried out in the network elements, thus decreasing the UE energy consumption significantly.

There are several technical enablers that make 5G radio networks capable of the features discussed above. Perhaps the most important one is the fact that 5G technologies are expected to be based on ultra-dense network (UDN) deployments where the access nodes (ANs) are distributed such that the inter-site distances are in the order of a couple of meters indoors and a couple of tens of meters outdoors [3]–[5]. This results in a situation where the UEs are most likely in line of sight (LoS) condition with one or multiple ANs at a time [10], [11]. Another very important aspect is that the ANs will most probably be equipped with smart antennas [3], such as antenna arrays and reconfigurable antennas, that allow for not only directional transmission and reception but also accurate spatial direction estimation. Thirdly, the signalling in the network will be based on frequent uplink (UL) pilot signals, transmitted towards the ANs by each of the UEs, hence making positioning possible in the network side [12], [13]. Finally, wider bandwidths at the existing and especially new frequency bands improve the accuracy of timing estimation, and thus improve also the ranging accuracy and positioning capabilities.

Whereas positioning will indisputably play a highly important role in the future society, in services like autonomous agricultural robots, packet delivery drones and highly automated factories, in this paper our focus is mainly on applications regarding cars and automotive transportation. On the one hand we will demonstrate how future 5G radio networks allow for ubiquitous high-accuracy positioning with a minimal energy consumption in the UEs, and on the other hand provide examples how the location-awareness can be exploited in upcoming traffic services such as self-driving cars and intelligent transportation systems (ITSs). In addition to pure

This work was supported by the Doctoral Program of the President of Tampere University of Technology, the Finnish Funding Agency for Technology and Innovation (Tekes), under the projects "5G Networks and Device Positioning", "TAKE-5: 5th Evolution Take of Wireless Communication Networks", and "Future Small-Cell Networks using Reconfigurable Antennas".

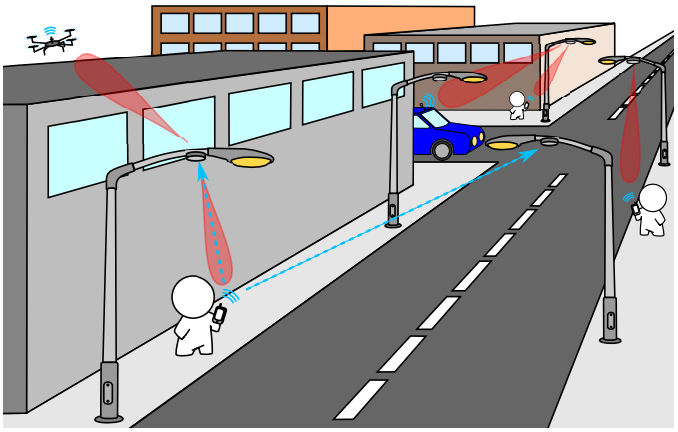

Fig. 1: Illustration of a 5G UDN where the ANs are attached to lamp posts, and UEs transmit periodical UL pilots towards the ANs. The UL pilots allow for ubiquitous positioning that is carried out in a network-centric manner.

real-time positioning and in contrast to the work in [13], we also analyze how accurately the location of a car can be predicted in the near future using various prediction numerologies and scenarios. Such information can be used, e.g., in proactive radio resource management (RRM) where the predicted location of a given UE can be utilized together with radio environment maps (REMs). This, in turn, allows, e.g., for proactive user scheduling and content prefetching, and thus provides remarkable improvements for the user quality of service (QoS) through seamless and transparent network functions.

The remaining of the paper is organized as follows. Section II introduces the network architecture as well as clock and channel models. Then, in Section III we shortly review the basic formulas of extended Kalman filter (EKF) and propose a solution for network-centric UE positioning, tracking and location prediction. Numerical performance analysis and discussion are subsequently given in Section IV. Finally, conclusions are drawn in Section V.

II. Network Architecture and System Model

A. 5G Network Architecture

Based on the focal 5G white papers [3]–[5], we consider 5G UDN where the ANs are deployed with a very high spatial density by attaching the ANs to lamp posts, see Fig. 1. Such a network structure results on an inter site distance (ISD) between ANs of around $50\,\mathrm{m}$, thus leading to a high LoS probability between the UEs and ANs. The height of the ANs is set to $7\,\mathrm{m}$ above the ground and each AN is equipped with an antenna array allowing for direction of arrival (DoA) estimation. The antenna arrays consist of 10 cylindrically-shaped dual-polarized cross-dipole antenna elements that are stacked in two layers. It is noteworthy that this is just an example of a possible antenna array geometry, and other type of arrays can be used as well. The locations of the ANs are denoted by $\mathbf{p}_{\ell_i} = [x_{\ell_i}, y_{\ell_i}, z_{\ell_i}]^{\mathrm{T}}$ where ℓ_i denotes the index of an AN. The AN locations are assumed to be known, e.g., by utilizing information from global positioning system (GPS).

According to the expectations of the 5G network functions, see, e.g., [12], [13], UEs transmit periodical UL pilot or beacon signals employing orthogonal frequency division multiplexing (OFDM) waveforms where the users are allocated to different subcarriers via the orthogonal frequency division multiple access (OFDMA) principle. Pilot signals are conventionally used for channel estimation, but now they are exploited also for network-centric positioning, thus allowing for a ubiquitous and "always-on" positioning solution. After receiving the pilots, the ANs detect whether or not they are in LoS condition with a UE. This can be carried out, e.g., by determining the Rice factor of the received signal strength (RSS) [14], which is typically 10-$20\,\mathrm{dB}$ in UDNs [11]. Based on the received pilot signals, each LoS-AN will subsequently estimate the directional and temporal parameters, i.e. DoA and time of arrival (ToA), of a UE, and communicate them to a central entity that carries out the 3D positioning.

B. Clock Models

In order to increase realism in the proposed positioning solution, the clocks within UEs and ANs are assumed to be mutually unsynchronized. In the considered network, the clock offset ρ_{UE} within a given UE is assumed to evolve according to the following time-varying clock model [15]

$$\rho_{\mathrm{UE}}[k] = \rho_{\mathrm{UE}}[k-1] + \Delta t \alpha_{\mathrm{UE}}[k] \tag{1}$$

$$\alpha_{\mathrm{UE}}[k] = \beta \alpha_{\mathrm{UE}}[k-1] + n[k], \tag{2}$$

where α_{UE} is the clock skew of a given UE at time instant k and Δt denotes a time-interval between consecutive time-instants $k-1$ and k. Furthermore, the driving noise of the clock skews is $n[k] \sim \mathcal{N}(0, \sigma_\alpha^2)$ and the constant parameter $|\beta| < 1$. In addition to the UEs, clocks within ANs are assumed to be phase-locked, i.e., the clock offset within an AN is not significantly varying over time. Finally, the nature of the aforementioned time-varying clock model allows for estimating the clock parameters of UE and LoS-ANs simultaneously with UE position within a single EKF. In this paper, all clock offsets are measured relative to a chosen reference AN.

C. Channel Model

We consider UL transmission from a single-antenna UE towards an AN with $\mathcal{M}_{\mathrm{AN}}$ antenna elements. In addition, we assume multicarrier OFDM waveforms with $\mathcal{M}_f$ active subcarriers. The multiantenna-multicarrier channel response vector $\mathbf{g}_{\ell_k} \in \mathbb{C}^{\mathcal{M}_{\mathrm{AN}}\mathcal{M}_f}$ can then be expressed as [16]

$$\mathbf{g}_{\ell_i} \approx \mathbf{B}_{\ell_i}(\theta, \varphi, \tau)\boldsymbol{\gamma} + \mathbf{n}, \tag{3}$$

where ℓ_i refers to an index of the i^{th} LoS-AN. Moreover, $\mathbf{B}_{\ell_i}(\theta, \varphi, \tau) \in \mathbb{C}^{\mathcal{M}_{\mathrm{AN}}\mathcal{M}_f \times 2}$ and $\boldsymbol{\gamma} \in \mathbb{C}^{2\times 1}$ are the polarimetric response of the AN ℓ_i and complex path weights, respectively. The model (3) is perturbed with complex-circular zero-mean white-Gaussian noise $\mathbf{n} \in \mathbb{C}^{\mathcal{M}_{\mathrm{AN}}\mathcal{M}_f \times 1}$ with variance σ_n^2.

The polarimetric antenna array response is equal to [16]

$$\begin{aligned}\mathbf{B}_{\ell_i}(\theta, \varphi, \tau) = [&\mathbf{G}_H \mathbf{d}(\varphi, \theta) \otimes \mathbf{G}_f \mathbf{d}(\tau), \\ &\mathbf{G}_V \mathbf{d}(\varphi, \theta) \otimes \mathbf{G}_f \mathbf{d}(\tau)],\end{aligned} \tag{4}$$

where $\otimes$ denotes the Kronecker product, and $\mathbf{G}_H \in \mathbb{C}^{\mathcal{M}_{\text{AN}} \times \mathcal{M}_a \mathcal{M}_e}$ and $\mathbf{G}_V \in \mathbb{C}^{\mathcal{M}_{\text{AN}} \times \mathcal{M}_a \mathcal{M}_e}$ are the effective aperture distribution functions (EADFs) for horizontal and vertical excitations, respectively. Numbers of the determined array response modes, i.e., spatial harmonics, in EADF are denoted as $\mathcal{M}_a$ and $\mathcal{M}_e$ for azimuth and elevation, respectively. Additionally, $\mathbf{G}_f \in \mathbb{C}^{\mathcal{M}_f \times \mathcal{M}_f}$ is the frequency response of the AN receivers, and $\mathbf{d}(\varphi, \theta) \in \mathbb{C}^{\mathcal{M}_a \mathcal{M}_e}$ is equal to

$$\mathbf{d}(\varphi, \theta) = \mathbf{d}(\theta) \otimes \mathbf{d}(\varphi) \tag{5}$$

where $\mathbf{d}(\varphi) \in \mathbb{C}^{\mathcal{M}_a}$ and $\mathbf{d}(\theta) \in \mathbb{C}^{\mathcal{M}_e}$ as well as $\mathbf{d}(\tau) \in \mathbb{C}^{\mathcal{M}_f}$ in (4) are Vandermonde structured vectors. These vectors carry out a mapping from the spatial/temporal parameters to the relative frequency domain such that

$$\mathbf{d}(\tau) = \left[e^{-j\pi(\mathcal{M}_f - 1) f_0 \tau}, \ldots, 1, \ldots, e^{j\pi(\mathcal{M}_f - 1) f_0 \tau}\right]^{\mathrm{T}}, \tag{6}$$

where f_0 stands for the OFDM subcarrier spacing. The formulation in (6) can be transformed to correspond also to $\mathbf{d}(\varphi)$ and $\mathbf{d}(\theta)$ by using the relation $\varphi/2 = \pi f_0 \tau$ (and similarly for ϑ). The array calibration data, represented using the EADF, can be determined, e.g., in an anechoic chamber [16]. In this paper, we assume that the EADFs are known for all ANs.

Note that the model in (3) is exploited by the DoA and ToA estimation and tracking algorithms described in Section III-B, and not employed for simulating the channel between the UE and ANs. In particular, an extensive ray-tracing tool is employed for generating the underlying multipath radio channel among UE and ANs [11], as described in more detail in Section IV.

III. Positioning Methods

A. Generic EKF Structure

Let us assume a system where the transition between two consecutive states $\mathbf{s}[k-1] \in \mathbb{R}^n$ and $\mathbf{s}[k] \in \mathbb{R}^n$ can be modelled with a linear state evolution model, whereas a relation between the state and available measurements $\mathbf{y}[k] \in \mathbb{R}^m$ can be written in non-linear form such that

$$\begin{aligned} \mathbf{s}[k] &= \mathbf{F}\mathbf{s}[k-1] + \mathbf{u}[k] \\ \mathbf{y}[k] &= \mathbf{h}(\mathbf{s}[k]) + \mathbf{w}[k], \end{aligned} \tag{7}$$

where $\mathbf{u}[k] \sim \mathcal{N}(0, \mathbf{Q})$ and $\mathbf{w}[k] \sim \mathcal{N}(0, \mathbf{R}[k])$. Let us further denote the *a priori* estimates as $\hat{\mathbf{s}}^-$ and $\hat{\mathbf{P}}^-$, and similarly the *a posteriori* estimates as $\hat{\mathbf{s}}^+$ and $\hat{\mathbf{P}}^+$. With this notation and assuming the models in (7), the predicted estimates of the state and its covariance at time step k can be written in the EKF prediction phase as

$$\hat{\mathbf{s}}^-[k] = \mathbf{F}\hat{\mathbf{s}}^+[k-1] \tag{8}$$

$$\hat{\mathbf{P}}^-[k] = \mathbf{F}\hat{\mathbf{P}}^+[k-1]\mathbf{F}^{\mathrm{T}} + \mathbf{Q}. \tag{9}$$

After the prediction phase, the *a priori* estimates can be updated using the latest measurements $\mathbf{y}[n]$ in the EKF update phase as

$$\mathbf{K}[k] = \hat{\mathbf{P}}^-[k]\mathbf{H}^{\mathrm{T}}[k](\mathbf{H}[k]\hat{\mathbf{P}}^-[k]\mathbf{H}^{\mathrm{T}}[k] + \mathbf{R})^{-1} \tag{10}$$

$$\hat{\mathbf{s}}^+[k] = \hat{\mathbf{s}}^-[k] + \mathbf{K}[k]\left[\mathbf{y}[k] - \mathbf{h}(\hat{\mathbf{s}}^-[k])\right] \tag{11}$$

$$\hat{\mathbf{P}}^+[k] = (\mathbf{I} - \mathbf{K}[k]\mathbf{H}[k])\,\hat{\mathbf{P}}^-[k], \tag{12}$$

where $\mathbf{H}[k]$ is the Jacobian matrix of the non-linear measurement model function $\mathbf{h}$ in (7), evaluated at $\hat{\mathbf{s}}^-[k]$.

B. DoA and ToA Estimation and Tracking

As shortly described in Section II-A, the periodically transmitted UL pilot signals are utilized for DoA and ToA estimation at each LoS-ANs before communicating and utilizing these estimates for positioning purposes in a central entity of the network. In this paper, we exploit the EKF-based solution proposed in [13] for DoA and ToA estimation and tracking due to its appealing properties such as relatively low computational complexity and high-accuracy estimation and tracking performance. In such a solution, the information form of the EKF is used instead of applying the Kalman gain form of the EKF presented in Section III-A. In general, the information form of the EKF is computationally attractive in cases where the dimension of the state is smaller than that of the measurement vector as well as when dealing with complex-valued data.

C. Proposed Positioning EKF

For the positioning EKF, which stems from the work in [13], two different UE motion models are considered for comparison purposes in this paper. The first model assumes that a given UE is moving with a nearly constant velocity (CV), whereas the second model considers a nearly constant acceleration (CA) for a given UE. In this section, only the CA model is presented whereas the considered CV model is the same as that in [13]. In particular, the state evolution and measurement models of the proposed positioning EKFs are assumed to follow the models in (7), where the state of the system for the CA model can be written as

$$\mathbf{s}[k] = \left[\mathbf{p}^{\mathrm{T}}[k],\, \mathbf{v}^{\mathrm{T}}[k],\, \mathbf{a}^{\mathrm{T}}[k],\, \rho_{\text{UE}}[k],\, \alpha_{\text{UE}}[k], \boldsymbol{\rho}^{\mathrm{T}}[k]\right]^{\mathrm{T}}, \tag{13}$$

where $\mathbf{p}[k] = [x[k], y[k], z[k]]^{\mathrm{T}}$, $\mathbf{v}[k] = [v_x[k], v_y[k], v_z[k]]^{\mathrm{T}}$, and $\mathbf{a}[k] = [a_x[k], a_y[k], a_z[k]]^{\mathrm{T}}$ are the 3D position, velocity, and acceleration of a given UE, respectively. Furthermore, $\rho_{\text{UE}}[k]$ and $\alpha_{\text{UE}}[k]$ denote the clock offset and clock skew of the UE at time-instant k, respectively. Since the proposed EKF is also capable of estimating and tracking the clock offsets of phase-locked LoS-ANs, these clock offsets $\boldsymbol{\rho}[k] = [\rho_{\ell_1}[k], \ldots, \rho_{\ell_{N_k}}[k]]^{\mathrm{T}}$ where N_k denotes the number of LoS-ANs at a time-instant k, are also included into the state vector. All the clock offsets are determined with respect to a predefined reference AN clock offset.

Moreover, assuming the CA motion model and the clock models in (1) and (2), the state transition matrix in (7) can be written in a block-diagonal form as

$$\mathbf{F} = \text{blkdiag}\left(\mathbf{F}_{\text{UE}}, \begin{bmatrix} 1 & \Delta t \\ 0 & \beta \end{bmatrix}, \mathbf{I}_{N_k \times N_k}\right), \tag{14}$$

where the second and third sub-matrices correspond to the clock evolution models of the UE and LoS-ANs, respectively. In addition, the sub-matrix $\mathbf{F}_{\text{UE}}$ in (14) for the considered CA model is

$$\mathbf{F}_{\text{UE}} = \begin{bmatrix} \mathbf{I}_{3\times3} & \Delta t\mathbf{I}_{3\times3} & \frac{\Delta t^2}{2}\mathbf{I}_{3\times3} \\ \mathbf{0}_{3\times3} & \mathbf{I}_{3\times3} & \Delta t\mathbf{I}_{3\times3} \\ \mathbf{0}_{3\times3} & \mathbf{0}_{3\times3} & \mathbf{I}_{3\times3} \end{bmatrix}, \tag{15}$$

The process noise covariance $\mathbf{Q}$ in the state evolution model in (7) can be also written in a block-diagonal form as

$$\mathbf{Q} = \text{blkdiag}\left(\mathbf{Q}_{\text{UE}}, \begin{bmatrix} \frac{\sigma_\eta^2\Delta t^3}{3} & \frac{\sigma_\eta^2\Delta t^2}{2} \\ \frac{\sigma_\eta^2\Delta t^2}{2} & \sigma_\eta^2\Delta t \end{bmatrix}, \sigma_\rho^2\mathbf{I}_{N_k\times N_k}\right), \tag{16}$$

where σ_η^2 is the variance of the clock skew driving noise of the UE clock, and σ_ρ^2 denotes the variance of the LoS-ANs clock offset noise processes. Furthermore, the sub-matrix $\mathbf{Q}_{\text{UE}}$ for the assumed CA model is

$$\mathbf{Q}_{\text{UE}} = \begin{bmatrix} \frac{\sigma_a^2\Delta t^5\mathbf{I}_{3\times3}}{20} & \frac{\sigma_a^2\Delta t^4\mathbf{I}_{3\times3}}{8} & \frac{\sigma_a^2\Delta t^3\mathbf{I}_{3\times3}}{6} \\ \frac{\sigma_a^2\Delta t^4\mathbf{I}_{3\times3}}{8} & \frac{\sigma_a^2\Delta t^3\mathbf{I}_{3\times3}}{3} & \frac{\sigma_a^2\Delta t^2\mathbf{I}_{3\times3}}{2} \\ \frac{\sigma_a^2\Delta t^3\mathbf{I}_{3\times3}}{6} & \frac{\sigma_a^2\Delta t^2\mathbf{I}_{3\times3}}{2} & \sigma_a^2\Delta t\mathbf{I}_{3\times3} \end{bmatrix}, \tag{17}$$

where σ_a^2 is the variance of the acceleration noise process.

In the proposed positioning EKF, the obtained measurements $\mathbf{y}[k] = [\mathbf{y}_{\ell_1}[k], \ldots, \mathbf{y}_{\ell_{N_k}}[k]]^{\text{T}}$, where individual measurements from an i^{th} LoS-AN $\mathbf{y}_{\ell_i}[k] = [\theta_{\ell_i}[k], \varphi_{\ell_i}[k], \tau_{\ell_i}[k]]^{\text{T}}$ are gathered, and related to the estimated state through the measurement model function $\mathbf{h}(\mathbf{s}[k]) = [\mathbf{h}_{\ell_1}(\mathbf{s}[k]), \ldots, \mathbf{h}_{\ell_{N_k}}(\mathbf{s}[k])]^{\text{T}}$, where

$$\mathbf{h}_{\ell_i}(\mathbf{s}[k]) = \begin{bmatrix} \arctan\left(\frac{\Delta y_{\ell_i}[k]}{\Delta x_{\ell_i}[k]}\right) \\ \arctan\left(\frac{\Delta z_{\ell_i}[k]}{\|\mathbf{p}[k]-\mathbf{p}_{\ell_i}\|_{2\text{D}}}\right) \\ \frac{\|\mathbf{p}[k]-\mathbf{p}_{\ell_i}\|_{3\text{D}}}{c} + (\rho_{\ell_i}[k] - \rho_{\text{UE}}[k]) \end{bmatrix}. \tag{18}$$

Here, the first two components correspond to the azimuth and elevation DoA, respectively, while the third one corresponds to the ToA measurements. Moreover, Δx_{ℓ_i}, Δy_{ℓ_i}, and Δz_{ℓ_i} denote the distances between the i^{th} LoS-AN and a given UE in x, y, and z directions, respectively, whereas $\|\mathbf{p}[k] - \mathbf{p}_{\ell_i}\|_{2\text{D}}$ and $\|\mathbf{p}[k] - \mathbf{p}_{\ell_i}\|_{3\text{D}}$ denote the 2D and 3D distances between the same LoS-AN and UE. Finally, the measurement model noise covariance matrix $\mathbf{R}[k]$ is defined using the uncertainties of the individual DoA and ToA estimates provided by the DoA and ToA tracking EKF such that $\mathbf{R}[k] = \text{blkdiag}(\mathbf{R}_{\ell_1}[k], \ldots, \mathbf{R}_{\ell_{N_k}}[k])$ [13].

In the considered position estimation and tracking EKF, the initialization procedure presented in [13] is employed in order to ensure necessary convergence in the beginning of the filtering. Using the aforementioned initialization method and the CA model as well as the CV model from [13], the EKF equations in III-A are now applicable. When the prediction performance of the proposed EKFs is evaluated, only the prediction phases, i.e., equations (8) and (9) are evaluated in the corresponding EKFs, and these *a priori* estimates are used as final state and covariance estimates.

IV. Numerical evaluations and analysis

A. Simulation Setup

In order to demonstrate and evaluate the performance of the proposed methods in terms of positioning and clock offset estimation accuracy in the outdoor METIS Madrid map environment [17], comprehensive numerical evaluations are carried out and analyzed in this section. For the evaluations, the METIS map-based ray-tracing channel model is implemented using uniform theory of diffraction (UTD) in order to model the propagation of received UL pilot signals [11] as realistically as possible. Furthermore, the transmit power of the tracked UEs is set to $10\,\text{dBm}$, and interfering UEs with the same transmit power are placed on the map randomly roughly $250\,\text{m}$ away from the UE with a density of $1000\,\text{interferers/km}^2$.

The considered 5G network is assumed to be operating in the $3.5\,\text{GHz}$ band and deploy OFDMA-based radio access with a $240\,\text{kHz}$ subcarrier spacing. The bandwith of the UL reference signals transmitted by the UEs, and used for positioning, is $5\,\text{MHz}$ and comprise of 20 subcarriers [12]. In addition, subframes of length $0.2\,\text{ms}$ containing 14 OFDM symbols are incorporated into the radio frame structure. Moreover, UL pilot signals of the UEs within a specific AN coordination area are assumed to be orthogonal through proper time and frequency multiplexing. In order to analyze the prediction performance of the positioning filters, prediction steps of the EKFs are carried out every $100\,\text{ms}$ while different time-intervals for fusing the obtained DoAs and ToAs from 2 LoS-ANs in the update steps of the EKFs are used.

In order to model the considered vehicular movement through random trajectories as realistically as possible, the motion of a reference UE is modeled using an empirical polynomial acceleration model [18] such that the velocity of a vehicle is 20-50 km/h. For the positioning and synchronization EKF, similar numerology for initializing the CV model parameters, the reference clock parameters of the UEs and ANs as well as the corresponding parameters within the EKF are used as in [19]. Moreover, the driving noise standard deviation σ_a in (17) is set to $0.1\,\text{m/s}^2$ in the considered positioning filters. In addition to the proposed DoA&ToA EKF, the performance of a more classical DoA-only EKF is also analyzed for comparison purposes in the next section.

B. Results and Discussion

Performance of the positioning filters is illustrated for the CV and CA motion models in Figs. 2a and 2b, respectively. There, the root mean squared error (RMSE) of 3D positioning is given as a function of the update time-interval (UTI). That is, the prediction steps of the filters are run in every $100\,\text{ms}$ in all cases, but the actual UTI is varying, thus illustrating positioning performance with different beaconing or pilot exploitation rates.

As expected, the overall positioning performance for both motion models degrades when UL pilots are exploited less frequently in the update phase of the EKFs as depicted in Figs. 2a and 2b. Interestingly though, higher than $2\,\text{m}$ positioning accuracy in terms of median RMSEs can be

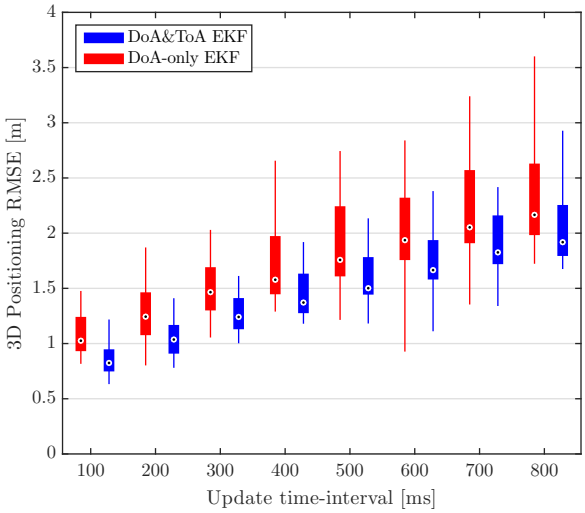

(a)

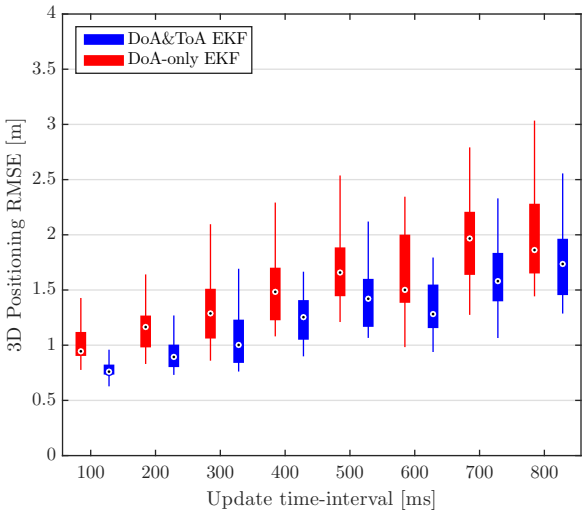

(b)

Fig. 2: Positioning RMSE with (a) CV and (b) CA motion models and different filter UTIs. Single prediction step is 100 ms in all cases. Circles symbolize the median values while the thicker lines highlight the results between the 25th and 75th percentiles. Moreover, the lengths of the thin lines equal 1.5 times the interquartile ranges.

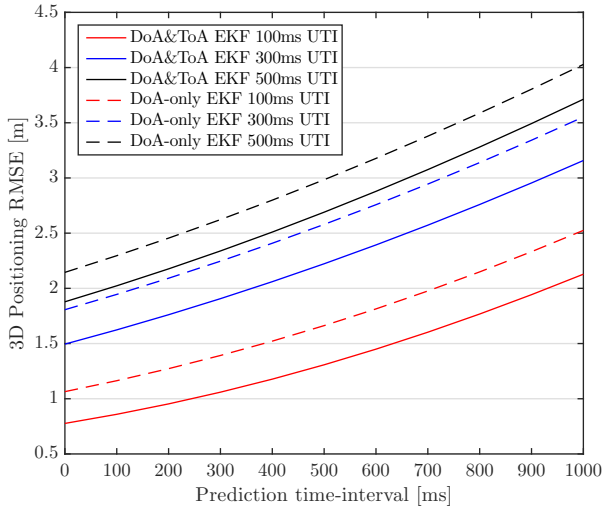

(a)

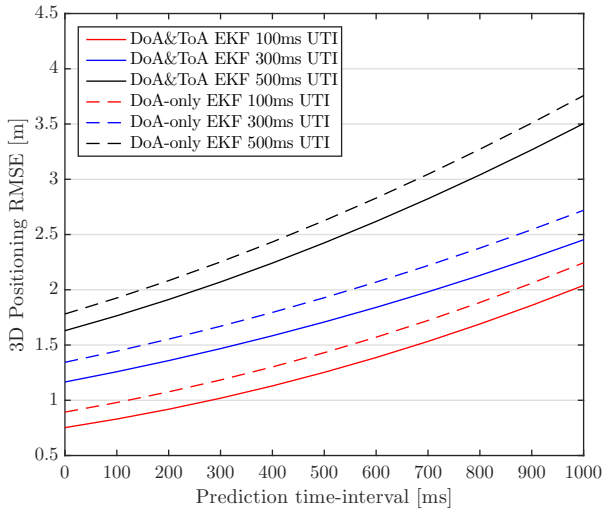

(b)

Fig. 3: RMSEs of instantaneous predicted UE locations with (a) CV and (b) CA motion models and different filter UTIs that are used before the actual location prediction phase has been started.

achieved with DoA&ToA EKFs with 100 ms prediction and 800 ms update intervals even under phase-locked network elements. Moreover, comparing the obtained results in Figs. 2a and 2b, the proposed CA-based EKF slightly outperforms the CV-based EKF, since the CA model typically allows for more accurate tracking of an object with acceleration variations. Finally, both DoA&ToA-based EKFs outperform the more classical DoA-only EKF in both motion model scenarios as expected.

Next we turn the focus on prediction of UE movement. In order to do that, we run multiple routes and realizations of moving UEs on the Madrid map, so that positioning filters are running until a random point on the route. On such a point, we start to predict the UE location within one second, while assuming that the UL pilot signals are no longer available. The RMSE of positioning as a function of time without UL pilot-based measurements is depicted in Figs. 3a and 3b, again for both CV and CA motion models, respectively.

Based on the obtained results in Figs. 3a and 3b, the proposed EKF that utilizes the CA model outperforms the CV-based EKF, while the performance of the DoA-only EKF is intuitively slightly worse than the proposed DoA&ToA EKFs. Moreover, the positioning RMSE increases as a function of the time elapsed after the last measurement step, but even the maximum RMSE after one second prediction is below 4 m. Interestingly, the lowest RMSE, which is obtained with the DoA&ToA EKF using 100 ms UTI and CA motion model, is only around 2 m after one second. When comparing this value with 13.9 m, the distance that a vehicle with 50 km/h velocity moves in one second, the prediction-based positioning algorithm provides obvious benefits in proactive network usage.

Finally, in order to visualize the statistical behavior of the case considered in Figs. 3a and 3b, we provide the cumulative

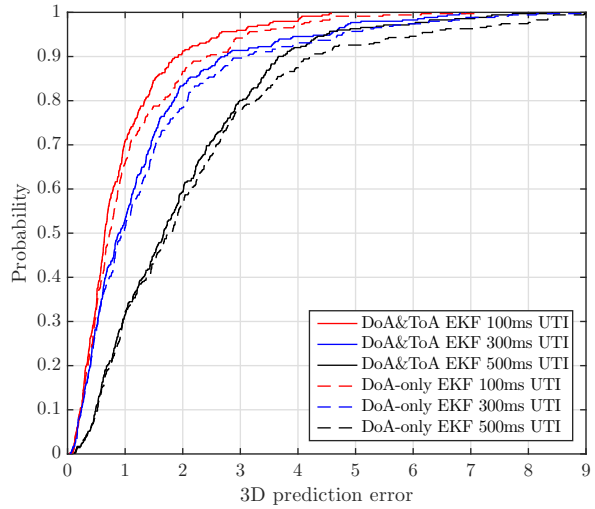

(a)

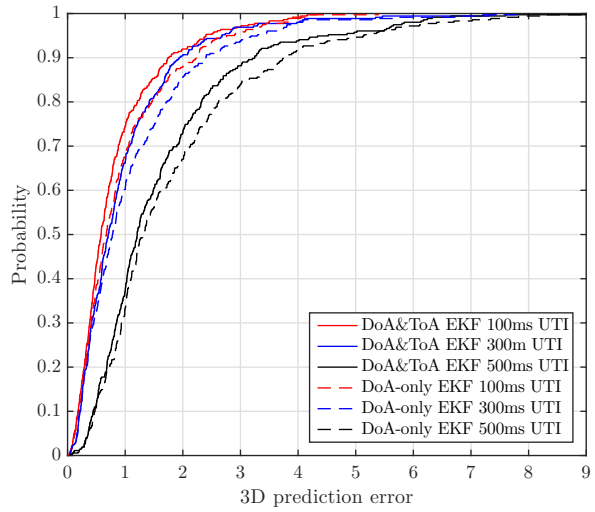

(b)

Fig. 4: Error distributions of predicted 3D locations at t=1 s with (a) CV and (b) CA motion models and different filter UTIs.

distribution functions (CDFs) of the error of prediction-based positioning at t =1 s, i.e., one second after the last measurement step, in Figs. 4a and 4b. The results show, again, that the CA motion model provides lower positioning errors than the CV counterpart, and that the exploitation of both DoA and ToA outperforms the DoA-only method. Considering now the CA motion model results with the DoA&ToA-based solution, we see that the positioning errors are smaller than 1.74 m, 1.94 m and 3.25 m for 90 % of the cases for UTIs being 100 ms, 300 ms and 500 ms, respectively. Consequently, the proposed methods can be considered as a valuable asset for future traffic solutions, being able to provide sub-meter range positioning for the current UE location and even predict short-time UE movement within an error of only couple of meters with a high probability, thus being at the same level or even better than the existing real-time positioning solutions.

V. Conclusions

In general, current and predicted location information of a UE can be utilized in future communication networks in order to enhance QoS, experienced by the users, in terms of proactive RRM and content prefetching, for example. In this paper, building on the premises of 5G UDNs, EKF-based positioning and synchronization solutions with two different UE motion models were described for estimating, tracking and predicting the UE locations. Thereafter, the performance of the proposed solutions were analyzed using extensive simulations and numerical evaluations in a realistic 5G vehicular scenario based on the METIS Madrid Map. The obtained results show that the proposed positioning solutions can provide sub-meter range positioning in networks, matching the 5G basic expectations. Additionally, we can even carry out short-time prediction of the user movement with a high probability, thus allowing for entirely new services that act in a proactive manner. Consequently, we foresee that radio-based network-centric positioning is likely to play a key role in future societies and especially in transportation related applications, such as self-driving cars and traffic flow control.

References

[1] A. Osseiran, F. Boccardi, V. Braun, K. Kusume, P. Marsch, M. Maternia, O. Queseth, M. Schellmann, H. Schotten, H. Taoka, H. Tullberg, M. Uusitalo, B. Timus, and M. Fallgren, "Scenarios for 5G mobile and wireless communications: the vision of the METIS project," *IEEE Commun. Mag.*, vol. 52, no. 5, pp. 26–35, May 2014.

[2] Huawei Technologies Co., "5G: New air interface and radio access virtualization," 2015. [Online]. Available: http://www.huawei.com/minisite/has2015/img/5g_radio_whitepaper.pdf

[3] 5G-PPP, "5G empowering vertical industries," Feb. 2015. [Online]. Available: https://5g-ppp.eu/wp-content/uploads/2016/02/BROCHURE_5PPP_BAT2_PL.pdf

[4] NGMN Alliance, "5G white paper," Mar. 2015. [Online]. Available: http://www.ngmn.org/5g-white-paper.html

[5] 5G Forum, "5G white paper: New wave towards future societies in the 2020s," Mar. 2015. [Online]. Available: http://www.5gforum.org/5GWhitePaper/5G_Forum_White_Paper_Service.pdf

[6] 3GPP TR 38.913, "Study on scenarios and requirements for next generation access technologies (V1.0.0)," Oct. 2016. [Online]. Available: http://www.3gpp.org/DynaReport/38913.htm

[7] D. Dardari, P. Closas, and P. Djuric, "Indoor tracking: Theory, methods, and technologies," *IEEE Trans. Veh. Technol.*, vol. 64, no. 4, pp. 1263–1278, Apr. 2015.

[8] J. Medbo, I. Siomina, A. Kangas, and J. Furuskog, "Propagation channel impact on LTE positioning accuracy: A study based on real measurements of observed time difference of arrival," in *Proc. IEEE PIMRC*, Sep. 2009, pp. 2213–2217.

[9] H. Liu, J. Yang, S. Sidhom, Y. Wang, Y. Chen, and F. Ye, "Accurate WiFi based localization for smartphones using peer assistance," *IEEE Trans. Mobile Computing*, vol. 13, no. 10, pp. 2199–2214, Oct. 2014.

[10] A. Dammann, R. Raulefs, and S. Zhang, "On prospects of positioning in 5G," in *Proc. IEEE International Conf. on Communication Workshop (ICCW)*, Jun. 2015, pp. 1207–1213.

[11] METIS, "D1.4 Channel models," Feb. 2015. [Online]. Available: https://www.metis2020.com/wp-content/uploads/METIS_D1.4_v3.pdf

[12] P. Kela, J. Turkka, and M. Costa, "Borderless mobility in 5G outdoor ultra-dense networks," *IEEE Access*, vol. 3, pp. 1462–1476, 2015.

[13] M. Koivisto, M. Costa, J. Werner, K. Heiska, J. Talvitie, K. Leppänen, V. Koivunen, and M. Valkama, "Joint device positioning and clock synchronization in 5G ultra-dense networks," accepted for publication in *IEEE Trans. Wireless Commun.*, in press, 2017.

[14] F. Benedetto, G. Giunta, A. Toscano, and L. Vegni, "Dynamic LOS/NLOS statistical discrimination of wireless mobile channels," in *Proc. IEEE VTC Spring*, 2007, pp. 3071–3075.

[15] H. Kim, X. Ma, and B. Hamilton, "Tracking low-precision clocks with time-varying drifts using Kalman filtering," *IEEE/ACM Trans. Netw.*, vol. 20, no. 1, pp. 257–270, Feb. 2012.
[16] A. Richter, "Estimation of radio channel parameters: Models and algorithms," Ph.D. dissertation, Ilmenau University of Technology, http://www.db-thueringen.de/servlets/DerivateServlet/Derivate-7407/ilm1-2005000111.pdf, 2005.
[17] METIS, "D6.1 Simulation guidelines," Oct. 2013. [Online]. Available: https://www.metis2020.com/wp-content/uploads/deliverables/METIS_D6.1_v1.pdf
[18] R. Akcelik and D. C. Biggs, "Acceleration profile models for vehicles in road traffic," *Transportation Science*, no. 1, pp. 36–54, Feb. 1987.
[19] M. Koivisto, M. Costa, A. Hakkarainen, K. Leppänen, and M. Valkama, "Joint 3D positioning and network synchronization in 5G ultra-dense networks using UKF and EKF," in *Proc. IEEE GLOBECOM Workshops*, Dec. 2016.